K. Rhee[1], M.H. Han[2], S.H. Cha[3], G. Khang[4]
[1] Department of Mechanical Engineering, Myongji University
[2] Department of Radiology, Seoul National University Hospital
[3] Department of Radiology, Choongbuk National University Hospital
[4]4 Department of Biomedical Engineering, Kyung Hee University

Abstract –

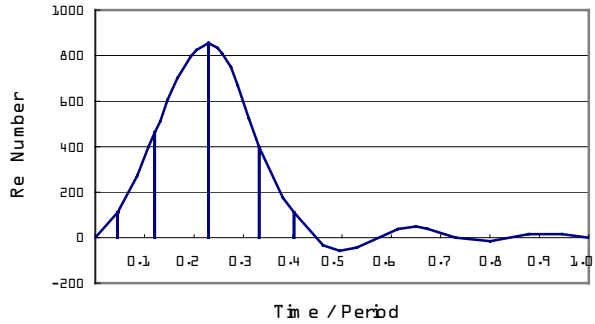

Fig. 1. Flow Waveform generated by a mock circulation loop. Vertical lines in the figure designate the instance of wall shear rate measurement.

I. Introduction

Aneurysm is a vascular disease characterized by bulging out of a segment of artery. Aneurysm is frequently found in abdominal artery, renal artery and cerebral arteries. Once it is formed, it may grow and rupture. The aneurysm found in the intracranial space is particularly dangerous since the rupture of intracranial aneurysm causes hemorrhage into subarachnoidal space. In order to treat aneurysm, surgical method of clipping the aneurysm neck has been applied. Because of high risk of surgical complications, endovascular techniques using coils, balloons and embolitic materials are currently used. Embolisation using coils is widely used in current days to treat the intracranial aneurysms. Micro coils are inserted into the aneurysm via micro catheter, and the coils inside the aneurysm sac reduce the blood flow, which causes thrombus formation and complete embolisation. Coil embolisation technique cannot be used in the aneurysm with wide neck (giant aneurysm and fusiform aneurysm) owing to the difficulties in complete filling of aneurysm sac and the risk of coil protrusion into the parent artery [1]. Recently, endovascular technique using a tubular shaped stent has been developed and successfully used in treating wide neck aneurysms [2,3]. Self-expandable stent is introduced via small catheter and placed at the aneurysm neck. A stent can promote thrombosis of aneurysm sac and the neointima formation of the stent wall can provide biocompatible passage of the parent artery. Thrombus formation involves various factors and complex mechanisms, and hemodynamics is believed to be one of the important factors responsible for thrombus formation. The insertion of a stent changes the flow characteristics such as flow stasis, the particle resident time and wall shear stress, which are believed to affect the thrombus formation inside the aneurysm sac. Lieber *et al* [4] qualitatively observed hemodynamic changes by stenting using laser induce fluorescence technique, and found the flow pattern changes by stent insertion. Yu and Zhao [5] measured steady velocity field in the stented sidewall aneurysm using a particle image velocitimeter, and found decreased velocities inside the aneurysm sac and wall shear stresses. In this study, we want to clarify the velocity and wall shear stress changes by stenting in fusiform aneurysm models under physiological flow waveform. The effects of stent porosity on the hemodynamics are also explored.

II. Method

A. Models and Test Rig

A fusiform aneurysm model was constructed from a rigid glass tube. In order to reduce the optical distortion caused by the round wall of a model, a silicone model was manufactured using the glass model as a male mold. The glass model was enclosed in the square box, and silicone (Sylgard 184, Dow–Corning Co.) resin was poured between a glass model and the square box. Once the silicone was cured, the glass model was taken out. The transparent silicone model has tube diameter of 5 mm, neck size of 15 mm and maximum aneurysm diameter of 9 mm. Stents of two different types were used. Stent, which is made of 0.1 mm diameter nitinol filaments, consists of a network of rhombus shape openings. The geometry of each stent is characterized by the porosity which is defined as the ratio

Report Documentation Page

Report Date	Report Type	Dates Covered (from... to)
25 Oct 2001	N/A	-

Title and Subtitle The Changes of Flow Characteristics Caused by A Stent in Fusiform Aneurysm Models	**Contract Number**
	Grant Number
	Program Element Number
Author(s)	**Project Number**
	Task Number
	Work Unit Number
Performing Organization Name(s) and Address(es) Department of Mechanical Engineering Myongii University	**Performing Organization Report Number**
Sponsoring/Monitoring Agency Name(s) and Address(es) US Army Research, Development & Standardization Group (UK) PSC 802 Box 15 FPO AE 09499-1500	**Sponsor/Monitor's Acronym(s)**
	Sponsor/Monitor's Report Number(s)

Distribution/Availability Statement
Approved for public release, distribution unlimited

Supplementary Notes
Papers from 23rd Annual International Conference of the IEEE Engineering in Medicine and Biology Society, October 25-28, 2001, held in Istanbul, Turkey. See also ADM001351 for entire conference on cd-rom. , The original document contains color images.

Abstract

Subject Terms

Report Classification unclassified	**Classification of this page** unclassified
Classification of Abstract unclassified	**Limitation of Abstract** UU

Number of Pages
3

of the effective opening area and the total area of each rhombus. The stents used in this study have the porosity of 0.86 and 0.79, and length of 20 mm. The aneurysm model was inserted into a mock circulation loop, which can generate physiological flow waveform. The flow loop consisted of pressure chamber, compliance chambers, resistant valves, constant head chamber, reservoir and circulation pump. Compressed air, which was controlled by a solenoid valve, was used to generate a pulsatile flow. The paraffin oil (kinematic viscosity 6 cS at 60°C) was used as the working fluid. The instantaneous flow rates were measured by an ultrasonic flow meter (TM 501, Transonic Inc.). The measured flow waveform is shown in Fig.1. The mean and peak Reynolds number was 200 and 900, respectively and the Womersley parameter was 2.5, which were similar to the flow parameters in the human carotid artery.

B. Flow Visualization

We used a flow visualization method incorporating photochromic dye in order to observe the flow fields. A photochromic dye shows photochromic behavior by changing its color by the excitation of light of an appropriate wavelength. We used TNSB (1',3',3'-trimethyl-6-nitroindoline-6-spiro-2-benzospyran) which could be excited by ultraviolet light wave. The transparent working fluid (TNSB - paraffin oil solution) was excited by a pulsed nitrogen laser (VSL 337ND, Laser Science Inc.), and a dark blue tracer line was generated along the path of laser beam. The movement of tracer line was captured by a progressive scan video camera (TM 9701, Pulnix Inc.). The captured image was enhanced using image processing software (Opimas, Bioscan Inc.), and the trailing edge of the tracer line was identified. Near wall (<0.5 mm from the wall) velocity profiles were calculated by dividing the tracer line displacements by the time interval between laser triggering and picture taking. Near wall velocity data were curve fitted to second order polynomials, and the wall shear rates were calculated form the velocity gradients at the wall. The details and accuracy of this technique is described elsewhere [6]. We could measure the wall shear rates at any instant of a flow cycle by synchronizing the laser and camera control signals to the solenoid valve signal which controlled on-off of pressurized air into the pressure chamber to generate the pulsatile flow in the circulation flow loop.

III. Results and Discussion

Flow fields were measured at five different locations along the aneurysm wall for five different phases of a flow cycle – early acceleration (t/T=0.046), mid acceleration (t/T=0.12), peak (t/T=0.23), early deceleration (t/T=0.33) and late deceleration (t/T=0.4). Fig. 2 shows the time line traces at peak flow. The straight vertical tracer line shows the path along which laser beam is passed through. The curved tracer lines show the displaced tracer lines which were straight 10 milliseconds ago. Since the flow field has axial and radial velocity components, the displaced tracer lines do not show the real velocity profiles. However, we

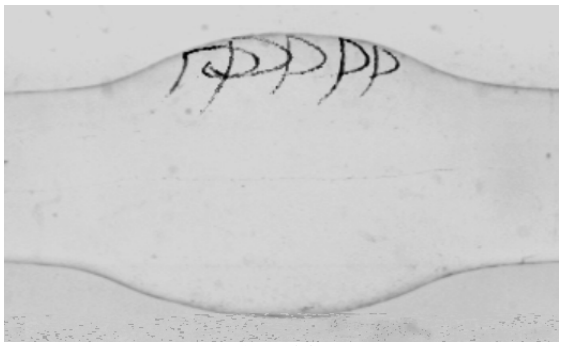

(a) Model 1

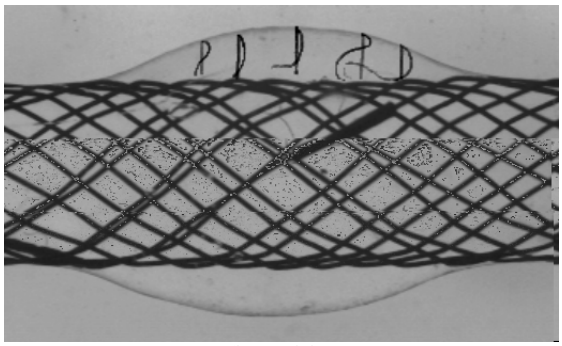

(b) Model 2

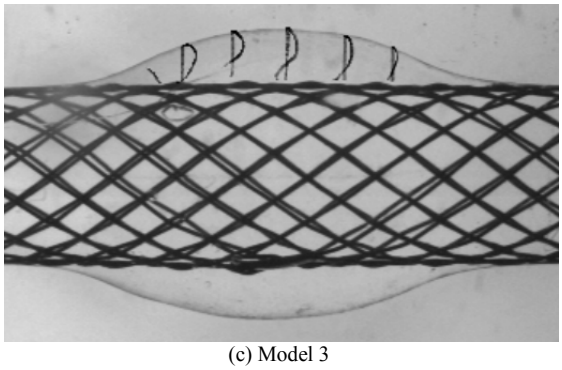

(c) Model 3

Fig. 2. Time line traces at peak flow for different models.

could qualitatively observed flow characteristics from the tracer line profiles. At a time when flow started to increase (t/T=0.046), the flow inside the aneurysm without a stent (model 1) moved right to left, which was a main flow direction. Similar flow patterns were shown in the aneurysm with a stent with porosity 0.86 (model 2) and a stent with porosity 0.79 (model 3). Near the peak flow, significant back flows were observed in model 1, which was consistent with the previous worker's result that large vortex was formed inside the aneurysm and the flow into aneurysm was introduced from the distal neck [4,5]. The flow field changes in the stented aneurysm models were significant. In both stented models, reverse flow was significantly reduced. Radial flow into aneurysm was dominant in the proximal neck in model 2 and in the distal neck in model 3. Comparing the flow fields in the non-stented model to the stented models, we could clearly see that a stent reduced the strong vortex motion inside the aneurysm and made the flow inside the aneurysm stagnant (Fig. 2). At a time of when flow diminished (t/T=0.4), vortex motion inside the aneurysm was disappeared in the non-stented aneurysm model while sluggish reverse flow was maintained in the stented aneurysm models. Wall shear

rates were calculated form the near wall velocity profile. The shear rates were significantly lower in the models with a stent except in early acceleration phase. All the models showed similar wall shear rate distributions in early acceleration phase. The shear rates in the model 1 was about three times higher in magnitude comparing to those in model 2 and 3 (Fig. 3) at peak flow. Shear rates distributions in the model 2 and 3 were slightly different, but the differences in magnitudes were small. Generally low and oscillatory shear stress provides favorable hemodynamic environment for intimal thickening. In order to quantify the oscillatory shear stress, oscillatory shear index (OSI) is defined by time integration of wall shear stress acting in the direction opposite to the mean flow divided by the time integration of the absolute value of wall shear stress during a period. Ku *et al* [7] showed the positive correlation between OSI and intimal thickening. Since we measured wall shear rate at five different phase of a flow cycle, OSI were approximated to the sum of absolute wall shear rates acting in opposite direction to the mean flow divided by the sum of the of absolute wall shear rates measured. OSI's were higher in the stented models at all measured locations (Table I).

IV. Conclusion

In order to clarify the hemodynamic changes caused by insertion of a stent, a flow visualization technique using photochromic dye was applied to the fusiform aneurysm models. The qualitative observation of tracer lines showed significant reduction of vortex motion in the stented aneurysm model. Also inflow patterns were different for three models. The non-stented model showed coherent inflow motion along the wall of the distal site of aneurysm, and a large vortex inside the aneurysm was formed. The stented models showed negligible inflow from the distal wall, and inflow were observed radially along the stent wall. Decreased inflow and vortex motion made the aneurismal flow stagnant, which might promote thrombus formation. Also significant reductions in wall shear rates were observed in the models with a stent. OSI's were higher at all measured locations with the stented models. Since reduced velocity, decreased wall shear rate and increased OSI can promote thrombus formation and intimal hyperplasia, we expect insertion of a stent provide favorable hemodynamic environment for aneurysm embolisation. The differences of flow patterns and wall shear rate distributions for stented models with different porosity were insignificant. This may result from the small difference of porosity in model 2 (0.86) and model 3 (0.79).

TABLE I
OSI'S AT FIVE DIFFERENT LOCATIONS OF ANEURYSM WALL
REFER THE LOCATIONS TO FIG. 3

Location	1	2	3	4	5
Model 1	0.06	0.12	0.11	0.16	0.18
Model 2	0.15	0.29	0.38	0.49	0.63
Model 3	0.27	0.16	0.12	0.31	0.36

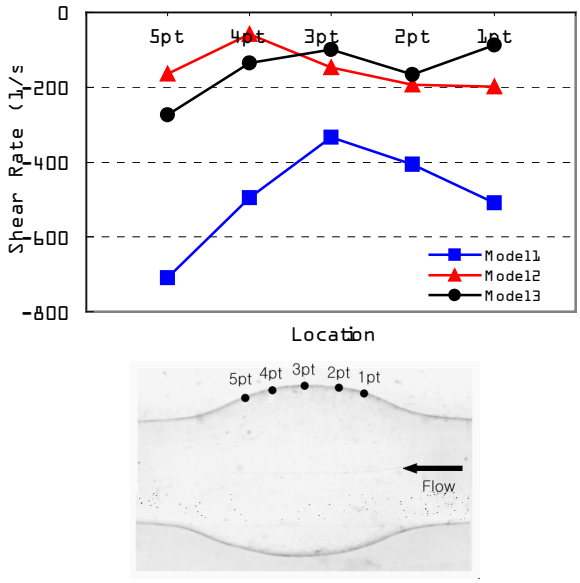

Fig. 3 Wall shear rate distributions along the aneurysm wall at peak flow. Lower figure shows the measurement locations.

Acknowledgment

This work was supported by grant No. 2000-2-20500-008-2 from the Basic Research Program of the Korea Science & Engineering Foundation.

References

[1] N. Knuckey, R. Haas, R. Jenkins, and M. Epstein, "Thrombosis of difficult intracranial aneurysms by the endovacular placement of platinum-dacron microcoils," *J Neurosurg.*, vol. 77, pp. 43-50, 1992

[2] M.P. Marks, M.D. Dake, G.K. Steinberg, A.M. Norbash, and B. Lane, "Stent placement for arterial and venous cerebrovascular disease: preliminary experience," *Radiology*, vol. 191, pp. 441-446, 1994

[3] A.K. Wakhloo, F. Schellhammer, J. de Vries, J. Haberstroh, and M. Schumacher, "Self-expanding and balloon-expandable stents in the treatment of carotid aneurysms: an experimental study in a canine model," *AJNR*, vol. 15, pp. 493-502, 1994

[4] B.B. Lieber, A.P. Stancampiano, and A.K. Wakhloo, "Alternation of hemodynamics in aneurysm models by tenting: influence of stent porosity," *Annals of Biomed Eng.*, vol. 25, pp. 460-469, 1997

[5] S.C.M. Yu and J.B. Zhao, "A steady flow analysis on the stented and non-stented side wall aneurysm models," *Medical Eng. & Physics*, vol. 21, pp. 133-141, 1999

[6] K. Rhee and J.M. Tarbell, "A study on the wall shear rate distribution near the end-to-end anastomosis of a rigid graft and compliant artery," *J. Biomech.* vol. 27, pp. 329-338, 1994

[7] D.N. Gu, D.D. Giddens, C.K. Zarins and S. Glagov, "Pulsatile flow and atherosclerosis in human carotid bifurcation," *Atherosclerosis*, vol. 5, pp.293-302, 1985